A Bio-designed Nanocomposite Biomaterial for Auricular Cartilage Reconstruction

Dr Leila Nayyer [a]

Dr Gavin Jell [a, b*]

Dr Ali Esmaeili [a, d]

Prof. Martin Birchall [b, e]

Prof. Alexander M. Seifalian [a,b]

[a]*Centre for Nanotechnology & Regenerative Medicine*, [b]*Division of Surgery and interventional science*, [c]*Institute of Biomedical Engineering*, [d]*The Ear Institute, University College London, London, WC1E 6BT, UK*

[e]*Department of Plastic and Reconstructive Surgery, Royal Free Hampstead NHS Trust Hospital, London, NW3 2QG, UK*

Corresponding Author(s):

Dr Gavin Jell

Lecturer of Nanotechnology & Regenerative Medicine

UCL Division of Surgery & Interventional Science

University College London

Email: g.jell@ucl.ac.uk

Tel: +44 20 7472 6144

Abstract

Current biomaterials for auricular replacement are associated with high rates of infection and extrusion. The development of new auricular biomaterials that mimic the mechanical properties of native tissue and promote desirable cellular interactions may prevent implant failure. A porous 3D nanocomposite scaffold (NS) based on POSS-PCU (a polycarbonate soft segment and a polyhedral oligomeric silsesquioxanes nanocage) was developed with an elastic modulus similar to native ear. *In vitro* biological interactions on this NS revealed greater protein adsorption, increased fibroblast adhesion, proliferation and collagen production compared with Medpor® (the current synthetic auricular implant). *In vivo* the POSS-PCU with larger pores (NS2; 150-250μm) had greater tissue ingrowth (~5.8× and ~1.4× fold increase) than the POSS-PCU with smaller pores (NS1; 100-50μm) and when compared to Medpor® (>100μm). The NS2 with the larger pores demonstrates a reduced fibrotic encapsulation compared with NS1 and Medpor® (~4.1× and ~1.6× fold respectively; $P<0.05$). Porosity also influenced the amount of neovascularisation within the implants, with no blood vessel observed in NS1 (12wks post-implantation). The lack of chronic inflammatory response for all materials may indicate that the elastic modulus and pore size of the implant scaffold could be important design considerations for influencing fibrotic responses to auricular and other soft tissue implants.

Keywords: biomaterial, auricular cartilage, nanocomposite scaffold, POSS-PCU, Medpor®

1. Introduction

Approximately 2 in 10,000 children are born with an ear deformity (e.g. including microtia and anotia), whilst traumatic injuries and malignant lesions (13% of all head and neck melanomas) add to the need for ear replacement and reconstruction.[1-3] Off-the-shelf synthetic auricular implants offer a number of advantages to routine autologous costal cartilage reconstruction surgery currently performed including; a reduced cost and length of operation, and no donor site morbidity.[4] Despite synthetic scaffolds being used for over 50 years in the auricular reconstruction surgery, they suffer from high failure rates. Medpor® auricular implants are the most commonly used auricular synthetic framework. Failure rates of between 11%-40% (depending on whether a temporoparietal fascia flap (TPFF) approach was used) have, however, been reported with the use of Medpor®.[5-7] There is, therefore, a real clinical need to develop improved biomaterials that are designed to have desirable biological interactions and reduced the failure rates.

The host tissue integration and vascularisation following implantation of auricular constructs depends upon both material surface properties (e.g. chemistry, topography, micro-mechanical properties) and bulk properties (e.g. pore size, porosity, and mechanical properties).[8-12] The material surface properties determine, the type, quantity and surface confirmation of protein interactions, which governs subsequent cellular interactions, which in turn may affect fibrotic encapsulation.[13] Fibrotic encapsulation has been previously reported as a cause of implant extrusion and failure.[14-16] Optimising these cell-material interactions may, therefore, reduce fibrotic encapsulation and failure rates of auricular implants.

Macrophages play an important part of the wound healing response when materials are implanted into tissues and express a large array of cytokines and chemoattractants, which modulate the behaviour of numerous cell types.[17-19] Macrophage behaviour can change

depending on the adsorbed protein and the material surface properties.[20-22] Ensuring that the biomaterial invokes a healing inflammation response, has the mechanical properties to resist unintentional wear and degradation and reduce implant fibrotic encapsulation is necessary for the long-term survival of the implants.

Neovascularisation is also vital for tissue regeneration and repair by supplying gases and nutrients for cells and tissues, and is a crucial parameter for supporting new tissue ingrowth in porous implants. Vascular endothelial growth factor (VEGF) is a key mediator for angiogenesis and granulation tissue formation in the early stage of healing,[23, 24] and can be expressed by fibroblasts within the peri-implant tissue. VEGF binds to its respective receptors, which are expressed on endothelial cells (ECs) and play important roles in transducing signals to induce angiogenesis *in vivo* through proliferation, migration and differentiation of ECs as well as regulates microvascular permeability.[25] Several studies have highlighted that an inadequate vascular supply and fibrous tissue ingrowth can be a cause of auricular implant failure due to the consequential flap ischemia or necrosis.[26-28] Indeed using vascularised grafts to completely covers the auricular Medpor® implants has significantly improved the short-term complication rates.[9]

Previous studies have developed a porous nanocomposite scaffold (NS), named polyhedral oligomeric silsesquioxane nanocage into polycarbonate based urea-urethane (POSS-PCU), for personalised auricular reconstruction using glass moulds and 3D-printing technology to replicate the shape of the original human auricle **(Figure 1)**.[29] We have also demonstrated that these NSs had an elastic modulus similar to native ear cartilage (5.7 MPa vs. 5.0 MPa), compared with Medpor® (141 MPa) **(Supplementary Table S1)**. Matching the elastic modulus of the native ear may be important in preventing elastic modulus mismatch between the scaffold and the surrounding tissue. A material considerably stiffer than the surrounding

tissue may cause micro-movement (when multilateral force is applied) and subsequently promote further fibrotic encapsulation, migration of the implant, and extrusion. Our simple approach is to create an "off-the-shelf" technology, whereby the scaffold matches and replaces the mechanical role of the ear cartilage and to improve the biological interactions of the scaffold with the surrounding dermal tissue. POSS-PCU has been also used successfully in first-in-man applications for replacement of coronary arteries, lacrimal ducts, and the world's first synthetic trachea.[30-32]

Here, we investigate the biological interactions of these NSs (compared to Medpor®) *in vitro* and *in vivo*, to assess the potential of the POSS-PCU NS as a substitute biomaterial implant for auricular cartilage replacement. The NS interaction with serum proteins, human dermal fibroblasts (HDFs) and macrophages were studied. The cellular behaviour, inflammatory and angiogenic response of the cells on these NSs were also investigated. To this end, the NS with two different pore sizes were subcutaneously evaluated *in vivo* in a rodent model for up-to 3 months, and compared with Medpor®.

2. Results and Discussion

2.1. In vitro evaluation of NS materials

Biomaterials designed for auricular reconstruction need to be able to support and maintain the auricular shape and be able to integrate with the sub-dermal layer. The materials properties (including surface chemistry, topography, mechanical properties, porosity and pore size) may be important in determining both 1) the initial material-cell interactions including initial protein adsorption, subsequent cell attachment and 2) inflammatory response, tissue ingrowth into the scaffold, ECM production and fibrous encapsulation. [33-38] Here we investigated if both these initial biological interactions and subsequent implant fibrotic encapsulation can be manipulated by the material physicochemical properties.

To compare protein adsorption on NS and Medpor®, we immersed them in foetal bovine serum protein media for 24 hrs. An increase in the total concentration of protein adsorption was observed between both samples, with NS showed the greatest total percentage of protein adsorption (76.16% ± 7.5 μg/ml), compared to Medpor® (43.00% ± 2.6 μg/ml) within 24 hrs **(Figure 2a)**. Protein absorption is both protein and substrate dependent and can be affected by the surface area (surface topographical features and porosity), as well as surface chemistry.[13, 39] Both scaffolds contain different porous structures (63.47%±1.35 total porosity in POSS-PCU & 50% total porosity in Medpor®) and different topographies (nano and microscale) **(Supplementary Table S1)**.[29] The increased surface area of the NS caused by the increase in porosity and nanoscale topography will provide a larger surface area for the serum proteins to be adsorbed than Medpor®. NS is also less hydrophobic (53.24±0.13º) than Medpor® (45.67±0.23º) **(Supplementary Table S1)**. The physiological effect of hydrophobicity on protein adsorption has been previously discussed, increased affinity between proteins and material surface may increase protein attachment but may also distort the original conformational of 3D protein structure, and thereby distort the cell receptor binding motifs and render them inactive.[40]

Increased adhesion of HDFs (human dermal fibroblasts) on NS was observed in the dynamic and static conditions, after 24 hrs culture, compared to Medpor® **(Figure 2b$_a$,b$_b$)**. The adhesion strength of cells in the native and continuous dynamic motion *in vivo* and the effects on wound healing and stability have been previously reported.[41] The increased cell adhesion on NS in both dynamic and static conditions could be explained by the increase in the adsorbed proteins and the increased surface area. The nanotopography of the NS may also have a direct effect on the adhesion strength of cells. Fibroblast filopodia number has been previously shown to increase on nano-featured surfaces compared to micro-featured

surfaces.[42, 43] In addition to increased cell attachment, NS also showed an increased number of cells and total metabolic activity over a 14 day culture period **(Figure 2c$_a$,c$_b$)** compared to Medpor®, although there was no difference in the rate of proliferation, and cell metabolic activity/µg DNA **(Figure 2c$_c$, Supplementary Figure 2)**. This suggests that number of cells on the scaffolds was proportional to the initial cell attachment. The increase in metabolic activity shown in this study is contrary to our previously study where we reported no difference in metabolic activity of carcinogenic (3T3) cell-line between Medpor® and NS surfaces,[29] this may be because the primary HDFs are more sensitive to environmental changes than the cancerous cells used previously.

The increased production of collagen hydroxyproline by HDF on NS compared to Medpor® (~2× fold, **Figure 2d$_a$**) may be due, in part, to the increased cell number **(Figure 2c$_a$)**. A higher collagen production/µg DNA **(Supplementary Figure 2)** was, however, observed and this could be due to the differences in the physicochemical properties of the scaffold (topography, surface chemistry etc), increased concentration of collagenic growth factors (e.g. TGFβ) in the media due to increased cell number, and/or increased juxtacrine signalling.[44, 45] The production of collagen is important for wound healing following invasive implantation, implant integration and tissue ingrowth, as well as to provide cell-signalling motifs (ligands) and growth factors for guiding cell behaviour.[19, 46] Prolonged expression or overproduction of specific type of collagen (Coll-1α) may, however, contribute to increased fibrotic encapsulation.[47, 48] Interestingly the increase of collagen hydroxyproline on NS was consistent with the reduced production of TNF-α cytokine, compared with Medpor® **(Figure 3d$_a$)**, which shown that the lowest level of this cytokine inhibit collagenase production.[49, 50]

There was no difference in total VEGF production of NS (269.2 ± 17.56 pg/ml) over time of

14 days (**Figure 2d$_b$**), compared with Medpor® (279.9 ± 25.58 pg/ml). A significantly higher VEGF production/μg DNA was, however, observed on Medpor® compared with NS (**Supplementary Figure2**). This increase could possibly be caused by the previously reported increase in VEGF production on stiffer surfaces.[51, 52]

Initial cytokine release profiles were also measured in an effort to evaluate if the different surfaces of NS and Medpor® scaffolds changed the behaviour of macrophages through the release of IL-1β, TNF-α, and IL-10 cytokines, which are important mediators of the inflammatory response and wound healing.[20] The total amount of both IL-1β and IL-10 released were similar for both NS and Medpor® at 72 hrs (**Figure 3c$_a$,e$_a$**). Macrophages cells attached to NS expressed lower total amounts of TNF-α (~2.4× fold) and lower TNF-α production/μg DNA (~2.7× fold) than on Medpor®, at 72 hrs (**Figure 3d$_a$, Supplementary Figure 3**). This may be caused by the increased expression of anti-inflammatory cytokine IL-10 than TNF-α on NS surfaces when compared to those expressed on Medpor® (**Figure 3a,b**), which inhibits the production of pro-inflammatory TNF-α cytokine, possibly via inhibition of NFκB activation.[53] Both IL-1β and TNF-α cytokines are essential for wound healing because they induce neutrophil recruitment, maturation and encourage angiogenesis. Prolonged expression or overproduction of these cytokines in the inflammatory phase may, however, cause granulation tissue formation and subsequently increased fibrotic encapsulation.[50, 54, 55] Interestingly the reduced pro-inflammatory TNF-α observed by macrophages on NS surfaces *in vitro* was consistent with a reduced thickness of the fibrotic capsule *in vivo*, compared to Medpor® (**Figure 3d$_a$, Figure 4c$_d$**).

Macrophage behaviour and subsequent inflammatory response can be affected by the surface chemistry and surface topography of the material.[53, 56-58] The inflammatory response (lower expression of TNF-α and IL-1β pro-inflammatory cytokines/μg DNA on NS surfaces

compared to Medpor®, **Supplementary Figure 3c$_a$,c$_b$**), may be due to differences in surface chemistry and topography between these materials **(Supplementary Table S1)**. The scale and spatial arrangement of the nano-topographical features on the nanocomposite scaffold may be partly responsible for this reduced pro-inflammatory response. Previous studies have shown that nanostructure features on titanium surfaces reduced the secretion of pro-inflammatory cytokines from macrophages.[22]

The increased expression of pro-inflammatory cytokines IL-1β/μg DNA and TNF-α/μg DNA **(Figure 3c$_b$,d$_b$,e$_b$)**, and reduced anti-inflammatory cytokine IL-10/μg DNA following endotoxin (LPS) challenge indicates that the macrophages can respond to inflammatory stimuli through NFκB activation pathway, and, hence, confirming that the scaffold autoclaving/cleaning technique is successful in removal of the majority of endotoxins.[59]

2.2 In vivo evaluation of NS implants

In vivo studies of the NSs made of two different pore sizes ranging from 50-100μm (NS1) and 150-250μm (NS2), but with a constant weight ratio of porogen particles to polymer was assessed by subcutaneous *in situ* implantation in the back of a rodent model, and compared with Medpor® (>100 μm). Here, the pore size of NSs was varied slightly to examine the effect of the changes on tissue ingrowth, angiogenesis and fibrotic response (which are not possible to measure *in vitro*). These pore sizes were chosen as an interconnective pore size of greater than 100 μm is required to accommodate a hierarchical vascular network within a scaffold,[60] with compromising the mechanical properties to native ear cartilage **(Supplementary Table S1)**.

On removal of the implants the scaffolds with the larger pore sizes (NS2 and Medpor®) were firmly anchored within the subcutaneous tissue compared to the NS1 (after a 12 wk implantation period, **Figure 4a$_a$,a$_c$**). The NS2 was, however, considerably harder to remove

than Medpor®. Possibly because the increased surface area encouraged greater cell/tissue infiltration as indicated with HE staining that showed NS2 and Medpor® with 68.70±5.85 % and 48.1±6.4 % fibrous tissue ingrowth, respectively, compared to NS1 (11.48±2.65 %) **(Figure 4b$_a$,b$_b$)**. This is also correlated with our earlier *in vitro* findings demonstrating that NS with a greater cellular adhesion and number by the increase in the adsorbed proteins and the increased surface area (surface topographical features, and porosity) **(Figure 2a,b$_a$,b$_b$,c$_a$,c$_b$)**.

A distinct variation in both the thickness and morphology (HE staining) of the fibrous capsule tissue was observed between the implants **(Figure 4c)**. In contrast to the largely avascular capsule with dense bundle of contractile microfilaments (elongated myofibroblasts and collagen fibers) seen around the smaller pore sized NS1 (**Figure 4c$_b$**, *white arrows*), a network of blood vessels was observed in the capsules surrounding the other NS2 of larger pores and Medpor® implants (**Figure 4c$_a$,c$_c$**, *black arrows*). Medpor® exhibited a thicker fibrosis capsule (96.43 ±16.02 μm) compared to NS2 of larger pores (**Figure 4c$_a$,c$_c$**, *white arrows,* 60.97 ± 16.07 μm). This thickening may be explained through the effect of increased substrate stiffness on myofibroblast formation, proliferation and collagen overproduction.[55, 61-63] The nanocomposite scaffolds have a more similar elastic modulus to the surrounding native ear tissue (compared to Medpor® implant) and may therefore reduce these phenomena **(Supplementary Table 1)**.[29] Softer substrates have been reported to reduce myofibroblast proliferation and the production of factors associated with fibrotic capsule formation (e.g. collagen type 1, α-smooth muscle actin (α-SMA)). [55] The poor cellular infiltration within the scaffolds with smaller pores (NS1) may also be contributing factor that prevents tissue embedded scaffold anchoring, thereby increasing interfacial micro-movement, and possibly contributing to inflammation and fibrotic capsule formation. A thicker capsule formation has

been previously reported on non-porous silicone scaffolds compared to the porous Medpor® for auricle replacement.[64] Pores beneath a certain size, may cause a similar response to no pores, whereby the fibrotic membrane does not "dip" into the scaffold pores but is continuous. This would allow a greater fibre alignment and thereby "force" emitted on the material (**Figure 4C$_b$**). The thickness and type of fibrous encapsulation may be important in the force submitted on the material, implant migration and possibly extrusion. Medpor® implants have been reported to have extrusion rates of 58% and 28%, within the rabbit and ovine auricular cartilage models, respectively.[65, 66]

The larger pore sizes of NS2 and Medpor® implants supported the formation of new internal blood vessels as early as 4 wks after implantation as evidenced by vWF (vascular EC marker) immunostaining (**Figure 5a$_a$,a$_b$**, *red arrows*). No evidence of microvascularisation was, however, seen within the smaller pore sizes of NS1 (**Figure 5a$_c$**). A scaffold with a pore size smaller than ~ 100 μm was previously demonstrated to have a decreased in vascularization, and subsequently tissue ingrowth and survival. [67] Semi-quantitative image analysis showed no significant differences in host tissue vascularization between the scaffolds with the larger pore size (Medpor® and NS2) in terms of mean microvessel size/μm^2 (**Figure 5a$_d$**), number of microvessel/mm^2, and total percentage microvessel area (mm^2) (**Supplementary Figure 5**). Microvasculature in the NS2 were, however, clearly present within the individual pores of the implant that crossing between pores (**Figure 5a$_a$,a$_b$**) compared to those in Medpor® (**Figure 5a$_a$,a$_b$**). Possibly advantage of neovascularization directly within the pores of the NSs could be the potential for a greater ability to integrate in the host environment. This is important because fibrovascular encasing of the implanted material is necessary for its anchorage in situ and for minimizing the occurrence of graft extrusion, as previously reported.[68-71]

The NS2 and Medpor® materials exhibited a similar inflammatory profile (both within the scaffold and within the fibrotic membrane), as determined by the average number of CD68+ cells/μm^2 (a pan specific macrophage/monocyte) (**Figure 5b$_a$,b$_b$**, *red arrows*). No $CD68^+$ cells present within the smaller pores of NS1 which probably a reflection of the lack of vascularity present in this scaffold (**Figure 5b$_c$**, *red arrows*). Number of CD68+ cells/μm^2 reduced over the 12 wks period following implantation ($P<0.05$), indicating no chronic inflammatory response for any of the implants (**Figure 5b$_d$**, *red arrows*). Although, some $CD68^+$ MNGCs (Multi-Nucleated Giant Cells) were present 12 wks post-implantation. Normal healing reactions without the chronic inflammatory response of these material implants was similar to that described in other animal models and in human using Medpor® implant.[65, 66, 72, 73]

As opposed to the more complicated and costly tissue engineering approaches, in this study, we have shown that biomaterials designed with appropriate mechanical stiffness, surface properties and porosity, can influence biological interactions including fibrotic encapsulation. The lack of a chronic inflammatory response (as shown here and previously reported for Medpor®), may indicate that either the model is not suitable for examining soft-tissue implant failure (e.g. duration of experiments, site of tissue or modelling micro-movement) or that the high failure/extrusion rates shown could be via a different non-inflammatory mechanism. Here we postulate that the type and size of fibrotic membrane formation surrounding the implants is important in determining extrusion rates and that the physicochemical properties of the implant scaffold (in particular the substrate stiffness) can be tailored to minimize this response.

3. Conclusion

Here we demonstrated that controlling the physicochemical properties of a biomaterial influences soft-tissue implant interactions (including fibrotic encapsulation) and can therefore lead to the design-led development of auricular implants that reduce failure rates. The *in vitro* and *in vivo* preclinical models used in this study provided, respectively, a setting to evaluate the clinical suitability and the subcutaneous behaviour of NSs, which had an elastic modulus closer to native ear cartilage (compared with the currently used auricular Medpor® implant). We demonstrated that NSs showed greater protein adsorption, and subsequently increased HDF adhesion (at both static and dynamic conditions), proliferation, and collagen production *in vitro*, compared to Medpor®. This was correlated to the *in vivo* findings, where the larger pore sized NS2 (150-250μm) demonstrate greater integration with the surrounding tissue, and a higher percentage of tissue ingrowth compared with both Medpor® and NS1 of smaller pores (50-100μm). At 12 wks post-implantation, significantly less fibrotic encapsulation was observed with elastic NS2 of large pores when compared with elastic NS1 of smaller pores and rigid Medpor® implants. The NS2 scaffold with larger pores of 150-250μm presented a promising alternative biomaterial for auricular reconstruction. The next stage will be focused on preclinical studies to fully establish the performance of 3D auricular scaffold made from this NS2 under GLP standards before embarking on clinical trials.

4. Experimental Section

Synthesis of Nanocomposite Polymer: POSS-PCU nanocomposite polymer was synthesised as described previously.[74] Briefly, polycarbonate polyol, 2000mwt and trans-cyclohexanechloroydrinisobutyl-Silsesquioxane (Hybrid Plastics Inc) were placed in a 500ml reaction flask equipped with mechanical stirrer and nitrogen inlet. The mixture was heated in order to dissolve the POSS cage into the polyol and then cooled to 70°C. Flake 4,4'-Methylenebis(phenyl isocyanate) (MDI) were added to the polyol blend and then reacted,

under nitrogen, at 75°C - 85°C for 90 minutes to form a pre-polymer. Dimethylacetamide (DMAC) was added slowly to the pre-polymer to form a solution; the solution was cooled to 40°C. Chain extension of the pre-polymer was carried out by the drop wise addition of a mixture of Ethylenediamine and Diethylamine in DMAC to form a solution of POSS modified Polycarbonate urea-urethane in DMAC. All the chemicals used in this study were received from Sigma-Aldrich Limited (Gillingham, UK).

Fabrication of Nanocomposite Scaffolds: NSs were synthesized and produced through optimized solvent evaporation and porogen leaching fabrication methods, as previously described.[29] The weight ratio of NaCl particles to POSS-PCU was controlled to 3:7 as with the previous studies. NSs with an average pore size of 150 μm, and a thickness of 700-800 μm, were cut into 16 mm diameter discs for use in 24 well plates, and used for *in vitro* cell culture experiments (n=4). Tissue culture plastic (TCP) used as control sample. The same NS discs (16mm in diameter), but with different thickness (~1.5 mm) and different pore sizes ranging from (50-100 μm) and (150-250 μm) were used for *in vivo* implantation (n=4 NS each time point). The pore size and morphology of these NSs was confirmed using scanning electron microscopy (SEM) **(Supplementary Figure 4)**. Micro thin Medpor® medical grade high-density porous polyethylene (HDPE) (Porex Surgical, Newnan, GA USA) (1.5 mm thickness sheets) with a manufacturer-specified pore size of larger than 100 μm and a pore volume of 50% were cut into circle-shaped disks (16 mm in diameter), and used for comparison (n=4 scaffolds each time point). Details of the physicochemical characterization of these NSs and Medpor® used in *in vitro* and *in vivo* were presented in Supplementary Information and methodology section **(Supplementary Table S1)**.

Protein Adsorption Studies: Protein adsorptions of scaffold surfaces were assessed using BCA kit (Bicinchoninic acid assay; Pierce™ thermo scientific, Rockford, IL USA), following the manufacturer's protocol. Polymer samples were prewetted in 70% ethanol for 30 min, and rinsed (x3) with PBS overnight under gentle shaking (25 rmp). Samples were then immersed in PBS supplemented with 20% fetal bovine serum proteins (FBS) for incubation periods of 24 hrs. After which samples washed (x4) with PBS, immersed for 1 hr in 1% sodium dodecyl sulphate in deionized H2O to retrieve adherent proteins in shaker, and incubated at 37 ºC for 30 min in working reagents. The absorbance eluted stain was measured using a colorimetric microplate reader (Anthos 2020) at 562 nm. Standard curves obtained from a series of dilutions of known standard bovine serum albumin (BSA) concentrations.

In vitro Biological Interactions: The interactions of HDFs with the NSs and Medpor® were assessed through cellular adhesion, proliferation, ECM collagen production and angiogenic response in this study. In order to determine the strength of cell adhesion on materials in a dynamic environment, total DNA using fluorescent Hoechst 33258 stain (Benzamide 33258, Sigma, UK), and Alamar Blue® (AB; Serotec Ltd, Kidlington, Oxford, UK) assays were performed at 24 hrs after initial cell seeding to determine the number of cells adhered on tested samples. Dynamic condition was performed using an orbital shaker (50 rpm) (Grant Bio PSU-10i; Wolf Laboratories Limited, York, UK), and optimised by a preliminary study examining the effects of different speeds (static, 50 rpm, 140 rpm, and 200 rpm) on adhesion of HDF cells seeded on TCP. Total DNA and AB assays were also used to determine the HDF proliferation and viability of the materials, respectively, on day 1, 3, 7, and 14 of culture. Total amount of extracellular secreted collagen (soluble and insolubilised) by HDF in the samples was measured on day 3, 7, and 14 using the hydroxyproline assay kit (QuickZyme Biosciences, Leiden, The Netherlands). The angiogenic response of HDF on

materials was also determined by release of VEGF quantification using a sandwich enzyme linked immunosorbent (ELISA; Quantikine, R&D System, Abingdon, UK) assay on day 3, 7, and 14 of culture. Macrophage responses to NSs and Medpor® were investigated by transformed U937 macrophage proliferation, cell morphology, and cytokines release assessments. Total DNA was performed on 24, and 72 hrs of culture to determine macrophage proliferation on materials **(Supplementary Figure3)**. Following day 3, macrophage morphology and adhesion on materials was determined using SEM **(Supplementary Figure3)**. Cytokines release including, IL-1β, TNF-a, and IL-10 quantification in response to material surfaces were assessed at 24, and 72 hrs using a sandwich ELISA assay (Quantikine, R&D System, Abingdon, UK). Samples with lipopolysaccharides (LPS) were used as positive controls. See Supplementary Information and the Methodology section for each individual test.

Rodent Animal Model and In vivo Evaluation: All procedures were conducted in accordance with protocols approved by the Royal Free Hospital (London, UK) on Animal Care. The experiments were conducted of eighteen adult male Sprague–Dawley rats (Charles River UK), weighing 250–400 g, were used for animal study. Each animal underwent implantation with two different material scaffolds from each three groups (NS1 (50-100μm), NS2 (150-250μm), and Medpor® (>100 μm)) in the dorsal subcutis of rats. Under aseptic technique and after shaving the subcutaneous pockets were made on each side of the midline into which each implant was placed through single incision. Each scaffold samples (n=4 per time point) were implanted subcutaneously at 1 cm from the site of incision. After 4, 8, and 12 wks, the implanted materials plus surrounding tissue were dissected from the subcutaneous pocket. Extracted samples (peri-implant tissue included) were labelled (orientation noted) and fixed in 10% (v/v) NBF before paraffin embedded for standard histology analysis to assess tissue

ingrowth and fibrous capsule thickness, and IHC to assess micro-neovascularisation and the host inflammatory responses using von Wilibrand Factor (vWFs) and CD68 staining, respectively (see Supplementary Information and the Methodology section). Thereafter, the animals were sacrificed by cervical dislocation.

Statistic: All quantitative data are presented as means ± standard deviation (SD). The differences between samples during repeated-measures testing was calculated by one-way or two-way analysis of variance (ANOVA) using Tukey's post hoc test, or two-tailed unpaired Student t-tests (for parametric data), with significance accepted at the 5% level using GraphPad Prism 6 Software.

Supporting Information

Supporting Information is available from the Wiley Online Library or from the author.

Acknowledgements

We acknowledge A. Darbyshire for polymer material synthesis. The authors would like to acknowledge the Northwick Park Hospital Institute for assistance in the *in vivo* histology and IHC staining works, and T. Jorgensenat from Falmouth University for use of the 3D printing facilities, and M. Durran for assistance in the glass mould design. This research was financially supported by a generous gift from Ms Hana Thalova to UCL Ear Institute and the Royal Free Hospital charity with HMRC No: X6243;

http://www.ucl.ac.uk/ear/research/microtia/gift.

Correspondence and requests for materials should be addressed to A.M.S.

The authors declare no competing financial interests in relation to the content of this paper.

Reference List

[1] N. H. Cox, S. K. Jones, R. M. MacKie, *Q*. *J*. *Med*. **1987**, *64*, 661.

[2] J. Harris, B. Kallen, E. Robert, *J Med*. *Genet*. **1996**, *33*, 809.

[3] D. V. Luquetti, E. Leoncini, P. Mastroiacovo, *Birth Defects Research Part A-Clinical and Molecular Teratology* **2011**, *91*, 813.

[4] Q. Zhang, R. H. Zhang, F. Xu, P. H. Jin, Y. L. Cao, *Plast*. *Reconstr*. *Surg*. **2009**, *123*, 849.

[5] T. Romo, III, L. G. Morris, S. D. Reitzen, S. N. Ghossaini, J. J. Wazen, D. Kohan, *Ann*. *Plast*. *Surg*. **2009**, *62*, 384.

[6] R. Cenzi, A. Farina, L. Zuccarino, F. Carinci, *J*. *Craniofac*. *Surg*. **2005**, *16*, 526.

[7] J. F. Reinisch, S. Lewin, *Facial Plast*. *Surg*. **2009**, *25*, 181.

[8] S. Lavenus, J. C. Ricquier, G. Louarn, P. Layrolle. *Nanomedicine (Lond)* **2010**, 5, 937.

[9] V. Karageorgious, D. Kaplan. *Biomaterilas*. **2005**, *26*, 5474.

[10] J. A. Henry, K. Burugapalli, P. Neuenschwander, A. pandit. *Acta Biomater*. **2009**, *5*, 29.

[11] B. Feng, Z. Jinkang, W. Zhen, L. Jianxi , C. Jiang, L. Jian. T. *Biomed Mater* **2011**, *6*, 015007.

[12] D. E. Discher, P. Janmey, Y. L. Wang. *Science* **2005**, *310*, 1139.

[13] C. J. Wilson, R. E. Clegg, D. I. Leavesley, M. J. Pearcy, *Tissue Eng* **2005**, *11*, 1.

[14] T. F. Henriksen, J. P. Fryzek, L. R. Holmich, J. K. McLaughlin, K. Kjoller, A. P. Hoyer, D. H. Olsen, S. Friis, *Annals of Plastic Surgery* **2005**, *54*, 343.

[15] R. C. Gerlach, D. R. Dixon, T. Goksel, J. T. Castle, W. A. Henry, *Oral Surgery Oral Medicine Oral Pathology Oral Radiology* **2013**, *115*, E44-E52.

[16] D. M. Tinsley, D. M. Betts. *Ophthalmol* **1994**, *4*, 77.

[17] L. A. DiPietro, *Shock* **1995**, *4*, 233.

[18] W. J. Kao, *Biomaterials* **1999**, *20*, 2213.

[19] Z. Xia, J. T. Triffitt, *Biomed*. *Mater*. **2006**, *1*, R1-R9.

[20] J. M. Anderson, A. Rodriguez, D. T. Chang, *Semin*. *Immunol*. **2008**, *20*, 86.

[21] T. O. Collier, J. M. Anderson, *J*. *Biomed*. *Mater*. *Res*. **2002**, *60*, 487.

[22] S. Lee, J. Choi, S. Shin, Y. M. Im, J. Song, S. S. Kang, T. H. Nam, T. J. Webster, S. H. Kim,

D. Khang, *Acta Biomater*. **2011**, *7*, 2337.

[23] S. Barrientos, O. Stojadinovic, M. S. Golinko, H. Brem, M. Tomic-Canic, *Wound*. *Repair Regen*. **2008**, *16*, 585.

[24] J. Li, Y. P. Zhang, R. S. Kirsner, *Microsc*. *Res*. *Tech*. **2003**, *60*, 107.

[25] N. Ferrara, W. J. Henzel, *Biochem*. *Biophys*. *Res*. *Commun*. **1989**, *161*, 851.

[26] H. Nakai, S. Ohmori, *Br*. *J*. *Plast*. *Surg*. **1979**, *32*, 261.

[27] P. K. Davis, S. M. Jones, *Br*. *J*. *Plast*. *Surg*. **1971**, *24*, 405.

[28] A. P. Sclafani, T. Romo, III, L. Silver, *Plast*. *Reconstr*. *Surg* **1997**, *99*, 41.

[29] L. Nayyer, M. Birchall, A. M. Seifalian, G. Jell, *Nanomedicine*. **2014**, *10*, 235.

[30] M. Ahmed, G. Hamilton, A. M. Seifalian, *Biomaterials* **2014**, *35*, 9033.

[31] K. Chaloupka, M. Motwani, A. M. Seifalian, *Biotechnol*. *Appl*. *Biochem*. **2011**, *58*, 363.

[32] P. Jungebluth, E. Alici, S. Baiguera, K. L. Blanc, P. Blomberg, B. Bozoky, C. Crowley, O. Einarsson, K. H. Grinnemo, T. Gudbjartsson, S. L. Guyader, G. Henriksson, O. Hermanson, J. E. Juto, B. Leidner, T. Lilja, J. Liska, T. Luedde, V. Lundin, G. Moll, B. Nilsson, C. Roderburg, S. Stromblad, T. Sutlu, A. I. Teixeira, E. Watz, A. Seifalian, P. Macchiarini, *Lancet* **2011**.

[33] X. Hu, K. G. Neoh, Z. Shi, E. T. Kang, W. Wang, *Tissue Eng Part A* **2013**, *19*, 1919.

[34] T. J. Webster, R. W. Siegel, R. Bizios, *Bioceramics* **2000**, *192-1*, 321.

[35] R. Johnson, D. Harrison, M. Tucci, A. Tsao, M. Lemos, A. Puckett, J. L. Hughes, H. Benghuzzi, *Biomed*. *Sci*. *Instrum*. **1997**, *34*, 47.

[36] L. Choritz, K. Koynov, G. Renieri, K. Barton, N. Pfeiffer, H. Thieme, *Invest Ophthalmol*. *Vis*. *Sci*. **2010**, *51*, 4047.

[37] K. R. Kam, L. A. Walsh, S. M. Bock, J. D. Ollerenshaw, R. F. Ross, T. A. Desai, *Tissue Eng Part A* **2014**, *20*, 130.

[38] B. S. Kopf, S. Ruch, S. Berner, N. D. Spencer, K. Maniura-Weber, *J*. *Biomed*. *Mater*. *Res*. *A* **2015**, *103*, 2661.

[39] P. Roach, D. Farrar, C. C. Perry, *J*. *Am*. *Chem*. *Soc*. **2006**, *128*, 3939.

[40] D. E. MacDonald, N. Deo, B. Markovic, M. Stranick, P. Somasundaran, *Biomaterials* **2002**, *23*, 1269.

[41] B. J. van Royen, S. W. O'Driscoll, W. J. Dhert, R. B. Salter, *Plast. Reconstr. Surg.* **1986**, *78*, 360.

[42] R. V. Goreham, A. Mierczynsk, L. E. Smith, R. Sedev, K. Vasilev, *Rsc Advances* **2013**, *3*, 10309.

[43] D. Guduru, M. Niepel, J. Vogel, T. Groth, *International Journal of Artificial Organs* **2011**, *34*, 963.

[44] T. A. Mustoe, G. F. Pierce, A. Thomason, P. Gramates, M. B. Sporn, T. F. Deuel, *Science* **1987**, *237*, 1333.

[45] Jell G, Minelli C, Stevens M, in *Fundemental of tissue engineering and regenerative medicine* (Eds: Meyer U, Meyer T, Handschel J, Wiesmann HP), Springer, Leipzig **2009**, 469.

[46] G. Brunner, R. Blakytny, *Thromb. Haemost.* **2004**, *92*, 253.

[47] S. J. Le, M. Gongora, B. Zhang, S. Grimmond, G. R. Campbell, J. H. Campbell, B. E. Rolfe, *Differentiation* **2010**, *79*, 232.

[48] K. R. Kam, L. A. Walsh, S. M. Bock, J. D. Ollerenshaw, R. F. Ross, T. A. Desai, *Tissue Engineering Part A* **2014**, *20*, 130.

[49] L. Jiang, Y. Dai, F. Cui, Y. Pan, H. Zhang, J. Xiao, F. U. Xiaobing, *Spinal Cord.* **2014**, *52*, 145.

[50] K. Rapala, M. Laato, J. Niinikoski, H. Kujari, O. Soder, A. Mauviel, J. P. Pujol, *European Surgical Research* **1991**, *23*, 261.

[51] C. Cha, J. H. Jeong, J. Shim, H. Kong, *Acta Biomaterialia* **2011**, *7*, 3719.

[52] K. Wang, R. C. A. Eguiluz, F. Wu, B. R. Seo, C. Fischbach, D. Gourdon, *Biomaterials* **2015**, *54*, 63.

[53] J. H. Silver, J. C. Lin, F. Lim, V. A. Tegoulia, M. K. Chaudhury, S. L. Cooper, *Biomaterials* **1999**, *20*, 1533.

[54] P. Shephard, G. Martin, S. Smola-Hess, G. Brunner, T. Krieg, H. Smola, *Am. J. Pathol.* **2004**, *164*, 2055.

[55] Z. Li, J. A. Dranoff, E. P. Chan, M. Uemura, J. Sevigny, R. G. Wells, *Hepatology* **2007**, *46*, 1246.

[56] M. A. Cardona, R. L. Simmons, S. S. Kaplan, *J. Biomed. Mater. Res.* **1992**, *26*, 851.

[57] W. G. Brodbeck, Y. Nakayama, T. Matsuda, E. Colton, N. P. Ziats, J. M. Anderson, *Cytokine* **2002**, *18*, 311.

[58] A. K. Refai, M. Textor, D. M. Brunette, J. D. Waterfield, *J. Biomed. Mater. Res. A* **2004**, *70*, 194.

[59] M. Ahmed, G. Punshon, A. Darbyshire, A. M. Seifalian, *J. Biomed. Mater. Res. B Appl.*

[60] B.D. Ratner, A.S. Hoffman, F.J. Schoen, J.E. Lemons (Eds.). *Biomaterials science: an introduction to materials and medicine*, *Elsevier*, *UK* **2004**.

[61] D. E. Discher, P. Janmey, Y. L. Wang, *Science* **2005**, *310*, 1139.

[62] P. D. Arora, N. Narani, C. A. G. McCulloch, *American Journal of Pathology* **1999**, *154*, 871.

[63] B. Hinz, *J. Invest Dermatol.* **2007**, *127*, 526.

[64] A. Shanbhag, H. I. Friedman, J. Augustine, A. F. von Recum, *Ann. Plast. Surg.* **1990**, *24*, 32.

[65] M. H. Hohman, R. W. Lindsay, I. Pomerantseva, D. A. Bichara, X. Zhao, M. Johnson, K. M. Kulig, C. A. Sundback, M. A. Randolph, J. P. Vacanti, M. L. Cheney, T. A. Hadlock, *Annals of Otology Rhinology and Laryngology* **2014**, *123*, 135.

[66] H. Neel, *Arch. Otolaryngol.* **1983**, *109*, 427.

[67] V. Karageorgios, D. Kaplan, *Biomaterials*. **2005**, *26*, 5474.

[68] K. Merritt, J. W. Shafer, S. A. Brown, *J. Biomed. Mater. Res.* **1979**, *13*, 101.

[69] P. A. Rubin, J. R. Bilyk, J. W. Shore, *Ophthalmology* **1994**, *101*, 1697.

[70] A. Berghaus, *Arch. Otolaryngol.* **1985**, *111*, 154.

[71] H. M. Rosen, *Plast. Reconstr. Surg.* **1991**, *88*, 1076.

[72] A. P. Sclafani, T. Romo, III, L. Silver, *Plast. Reconstr. Surg* **1997**, *99*, 41.

[73] A. Shanbhag, H. I. Friedman, J. Augustine, A. F. von Recum, *Ann. Plast. Surg* **1990**, *24*, 32.

[74] R. Y. Kannan, H. J. Salacinski, M. Odlyha, P. E. Butler, A. M. Seifalian, *Biomaterials* **2006**, *27*, 1971.

Figure Legends

Figure 1. Design and construction of a porous auricular framework and *in vitro* and *in vivo* testing of its properties in a 3-D circle-shaped disc. **a**, Standard triangulate language (STL) files format taken from a CT scan data of the external part of a human ear model is sliced into thinner horizontal layers of powder, and solidified by a binder using, **b**, an additive layer manufacturing (ALM) software. **b**, Positive 3-D printing auricle mould using ALM based on powder bed and inkjet 3D printing is used, to design a, **c**, negative ear glass-mould to construct a, **d**, auricular POSS-PCU nanocomposite scaffold through a solvent evaporation/porogen leaching fabrication technique. $\mathbf{d}_{a}$, SEM cross-sectional of the porous nanocomposite scaffold, and $\mathbf{d}_{b}$, a schematic diagram of the chemical structure of poly-oligomeric silsesquioxane (POSS) nanocages.

Figure 2. *In vitro* biological evaluation of HDFs of the NSs compared to Medpor®. a, A significantly lower level of protein adsorption was observed on Medpor® compared with NS at 6 and 24 hrs. $\mathbf{b}_{a}$, and $\mathbf{b}_{b}$**,** A significantly higher percentage of metabolic activity and number of HDFs attached on NS compared to Medpor® after 24 hrs at dynamic and static culture (relative to TCP %). $\mathbf{c}_{a}$, higher HDFs number and $\mathbf{c}_{b}$**,** higher metabolic activity were presented on NS compared with Medpor® at day 7 and 14. $\mathbf{c}_{c}$, No significant differences in cell proliferation rate were observed between the scaffolds after 14 days of culture (% of total DNA relate to day 1). $\mathbf{d}_{a}$, A significantly higher amount of collagen production was found on NS over 14 days culture. $\mathbf{d}_{b}$, no significant difference in level of VEGF production was observed between both scaffolds over 14 days. $*P < 0.05$, errors bar=SD, (n=4, scaffolds in each group at each time-point).

Figure 3. *In vitro* inflammatory responses of macrophages of the NSs compared to Medpor®. a, POSS-PCU surfaces expressed a significant increase in IL-10 concentration by U937 cells after 72 hrs into the supernatants, and showed a highest level of IL-1β and IL-10 respectively, and a lowest level of TNF-α cytokines production on both 24 and 72 hrs culture. **b,** Medpor® surfaces also expressed a significant reduction in IL-1β, and a significant increase in IL-10 concentrations after 72 hrs culture

into the supernatants, and presented a highest level of IL-1β cytokines production compared to the other two cytokines on both 24 and 72 hrs. **c_a, d_a,** and **e_a**, No significant differences in IL-1β and IL-10 production were observed between the two scaffolds during 72 hrs period. However, a significant increase in TNF-α was found on Medpor®. **c_b, d_b,** and **e_b**, LPS treatment resulted in a significant increased in pro-inflammatory IL-1β and TNF-α cytokines production/μg DNA, but not anti-inflammatory IL-10 cytokine on both scaffold surfaces at 72 hrs. **P* < 0.05, errors bar=SD, (n=4, scaffolds in each group at each time-point). Scale bar 20 μm.

Figure 4. *In vivo* tissue ingrowth and fibrotic encapsulation evaluation of the NSs implants in rats compared to Medpor®. a, Observation on retrieval of implanted materials at 12 wks subcutaneous post-implantation in the rat model. All implanted materials preserved their pre-implanted round shapes. **a_a**, POSS-PCU (150-250μm; NS2) and, **a_c**, Medpor® were firmly anchored within the subcutaneous tissue (*white arrows*), but **a_b**, POSS-PCU (50-100μm; NS1) were loosely attached with the surrounding soft tissue (*white arrow*). **b**, Fibrous tissue ingrowth within all the implanted materials demonstrated by, **b_a**, a H&E evaluation and **b_b**, a percentage volume fraction of fibrous tissue representing the proportion of total scaffold volume (*area between white dash lines*) occupied by fibrous tissue at 4, 8, and 12 wks. Scale bars represent 500 μm. **P* < 0.05, errors bar=SD. **c**, Fibrous encapsulation of all the scaffolds at 12 wks post-implantation presented by, **c_a**, a H&E evaluation and, **c_b**, a semi-quantitative histological analysis of fibrous capsule thickness (*white arrows*) around the implants. The tissue-implant interface where the capsule not attached to POSS-PCU of smaller pores (*blue asterisk*). Some blood vessels surrounded the implants (*black arrows*). Scale bars represent 100 μm. (n=4 scaffolds in each group at each time point).

Figure 5. *In vivo* neovascularisation and host macrophage responses evaluation of the NSs implants compared to Medpor®. a, Endothelial staining with vWFs IHC (*red arrows*) revealed vessel lumens area of 12 wks observed within, **a_a**, POSS-PCU (150-250μm; NS2), **a_b**, Medpor®, but not on, **a_c**, POSS-PCU (50-100μm; NS1) implants. **a_d**, A measured mean microvessel size/μm^2 in

large pore sizes of POSS-PCU and Medpor® implants, representing the size of blood vessels within grown tissue per scaffold, as quantified at 4, 8, and 12 wks, with no observable significant differences between the groups. **b**, Pan-macropahge/monocyte staining with CD68 IHC (*red arrows*) of 12 wks observed in host tissue across and within, $\mathbf{b_a}$, POSS-PCU (150-250μm; NS2) and, $\mathbf{b_b}$, Medpor®, and, $\mathbf{b_c}$, surrounding POSS-PCU (50-100 μm; NS1) implants (but no sign of CD68 positive staining within the implants). $\mathbf{b_d}$, Quantitative IHC represented a significantly reduced average number of positive macrophage cells across and within the POSS-PCU of smaller pores compared with other scaffolds per field of view area, at all time points. $*P < 0.05$, errors bar=SD, (n=4, scaffolds in each group at each time-point). Scale bars 50 μm.

Figure 1.

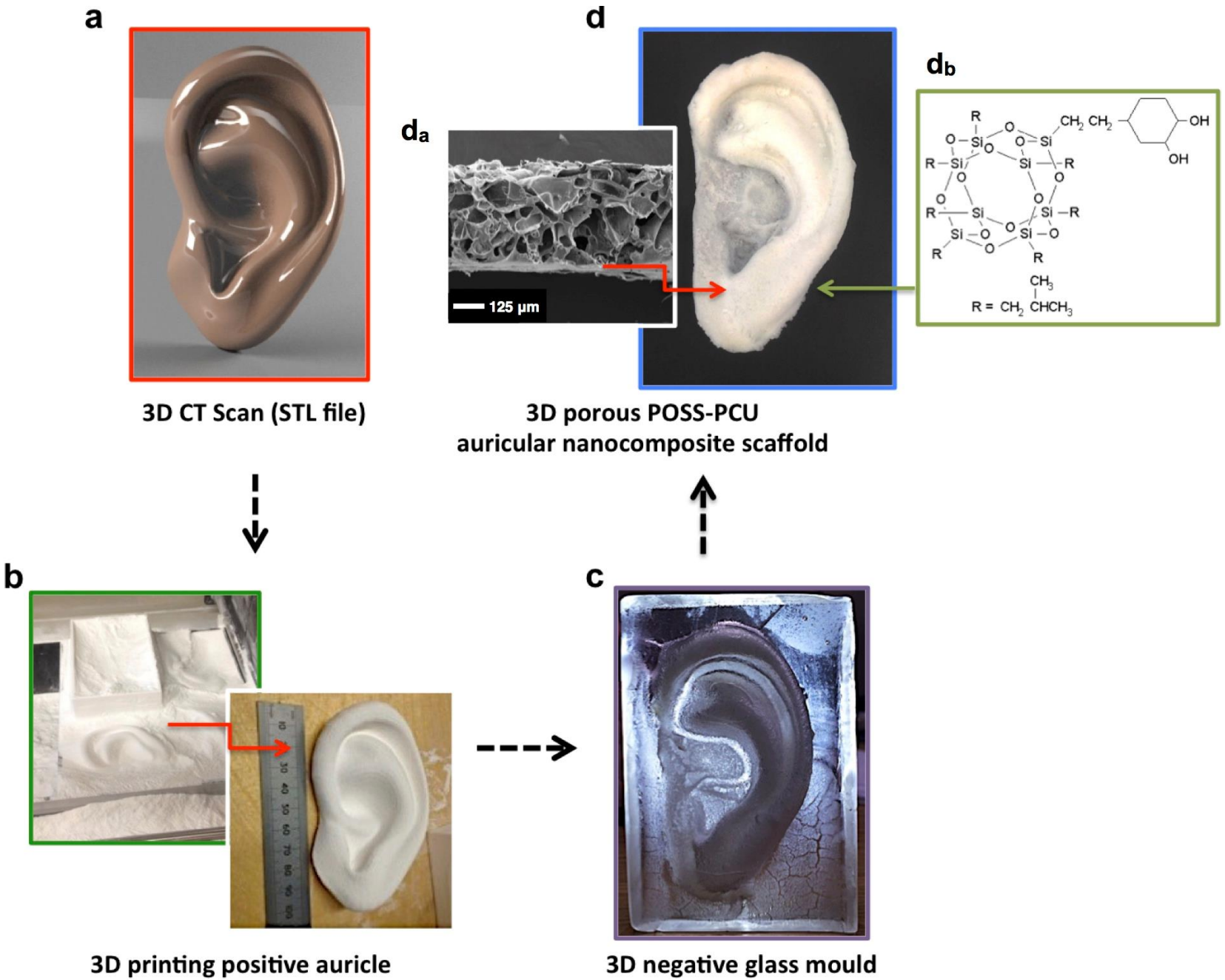
a
3D CT Scan (STL file)
d
da
125 µm
db
3D porous POSS-PCU
auricular nanocomposite scaffold
b
3D printing positive auricle
c
3D negative glass mould

Figure 2.

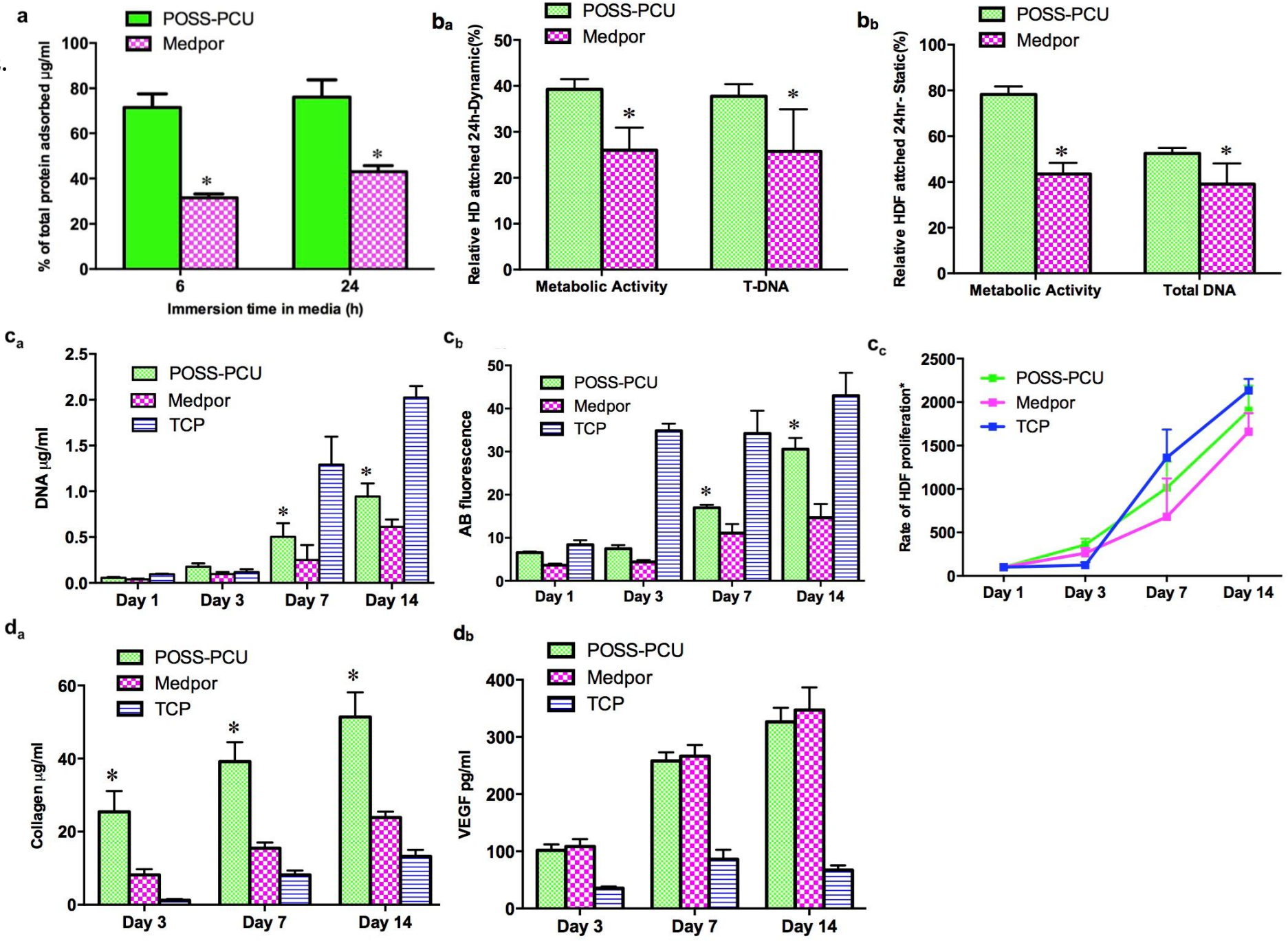
a
POSS-PCU
Medpor
% of total protein adsorbed µg/ml
Immersion time in media (h)
6
24
ba
Relative HD attched 24h-Dynamic(%)
Metabolic Activity
T-DNA
bb
Relative HDF attched 24hr- Static(%)
Metabolic Activity
Total DNA
ca
TCP
DNA µg/ml
Day 1
Day 3
Day 7
Day 14
cb
AB fluorescence
cc
Rate of HDF proliferation*
da
Collagen µg/ml
db
VEGF pg/ml

Figure 3.

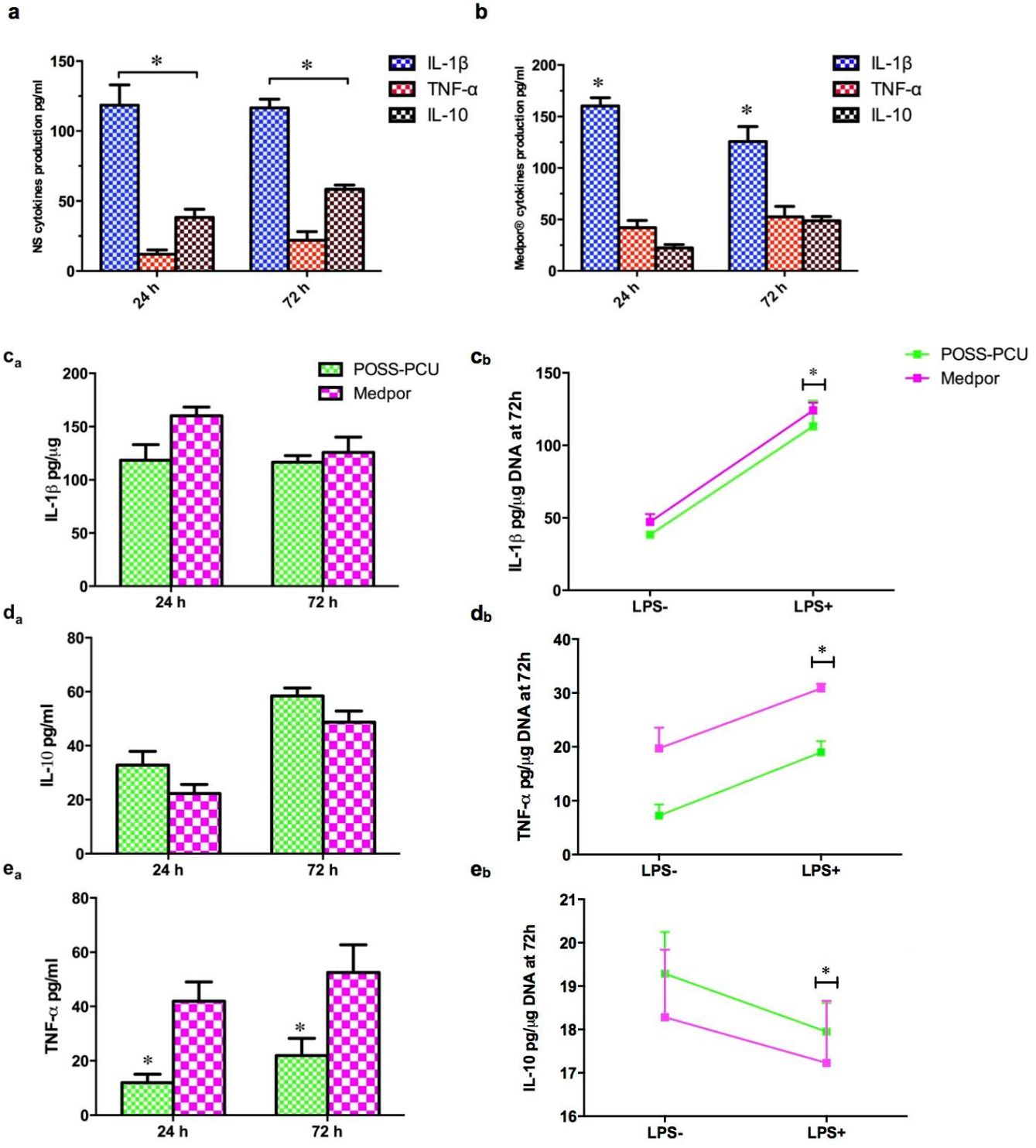
a
NS cytokines production pg/ml
150
100
50
0
*
*
IL-1β
TNF-α
IL-10
24 h
72 h
b
Medpor® cytokines production pg/ml
200
150
100
50
0
*
*
IL-1β
TNF-α
IL-10
24 h
72 h
ca
IL-1β pg/μg
200
150
100
50
0
POSS-PCU
Medpor
24 h
72 h
cb
IL-1β pg/μg DNA at 72h
150
100
50
0
*
POSS-PCU
Medpor
LPS-
LPS+
da
IL-10 pg/ml
80
60
40
20
0
24 h
72 h
db
TNF-α pg/μg DNA at 72h
40
30
20
10
0
*
LPS-
LPS+
ea
TNF-α pg/ml
80
60
40
20
0
*
*
24 h
72 h
eb
IL-10 pg/μg DNA at 72h
21
20
19
18
17
16
*
LPS-
LPS+

Figure 4.

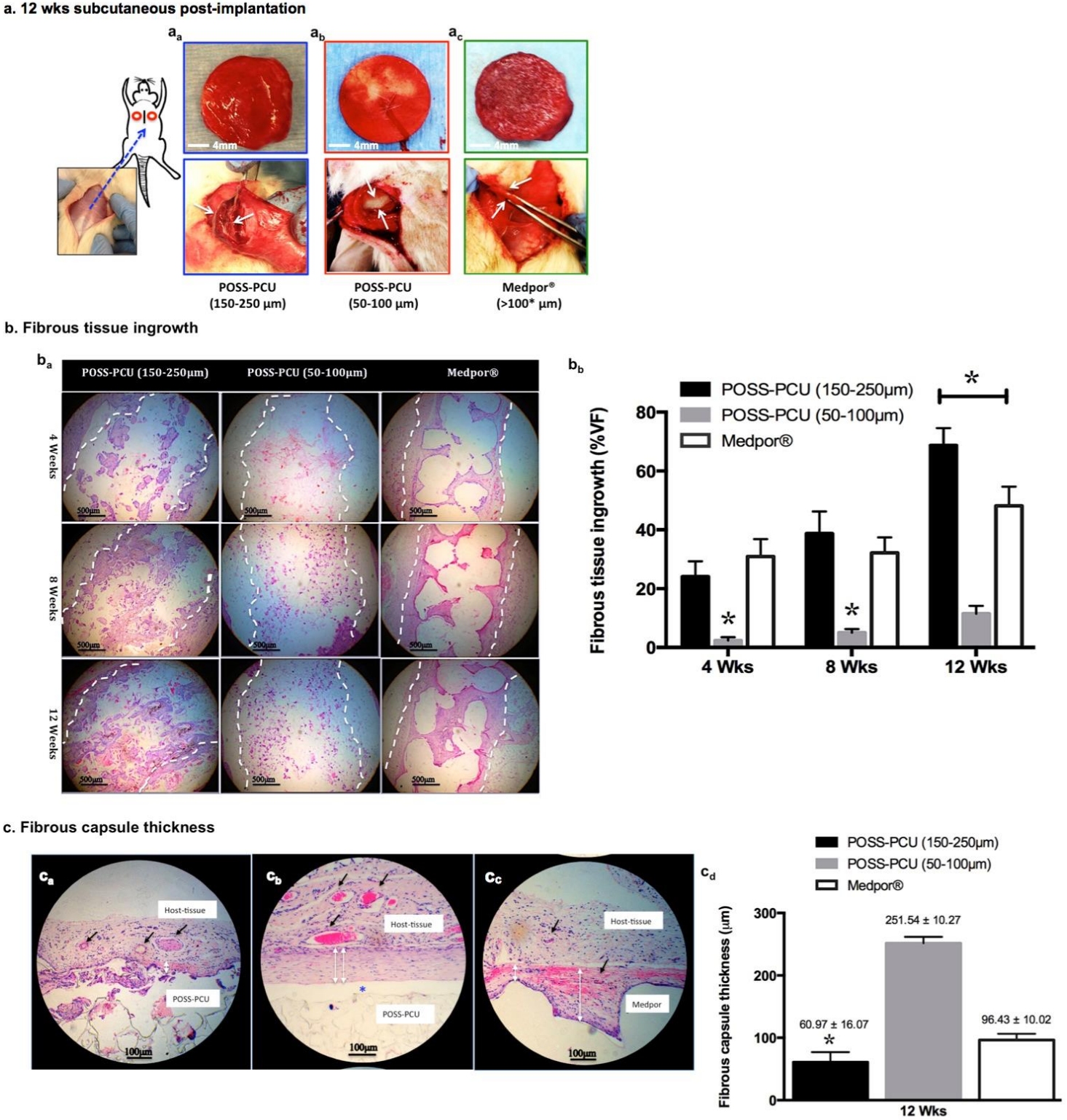
a. 12 wks subcutaneous post-implantation
a_a
a_b
a_c
4mm
POSS-PCU (150-250 µm)
POSS-PCU (50-100 µm)
Medpor® (>100* µm)
b. Fibrous tissue ingrowth
b_a
POSS-PCU (150-250µm)
POSS-PCU (50-100µm)
Medpor®
4 Weeks
8 Weeks
12 Weeks
500µm
b_b
Fibrous tissue ingrowth (%VF)
4 Wks
8 Wks
12 Wks
c. Fibrous capsule thickness
c_a
c_b
c_c
Host-tissue
POSS-PCU
Medpor
100µm
c_d
Fibrous capsule thickness (µm)
60.97 ± 16.07
251.54 ± 10.27
96.43 ± 10.02
12 Wks

Figure 5.

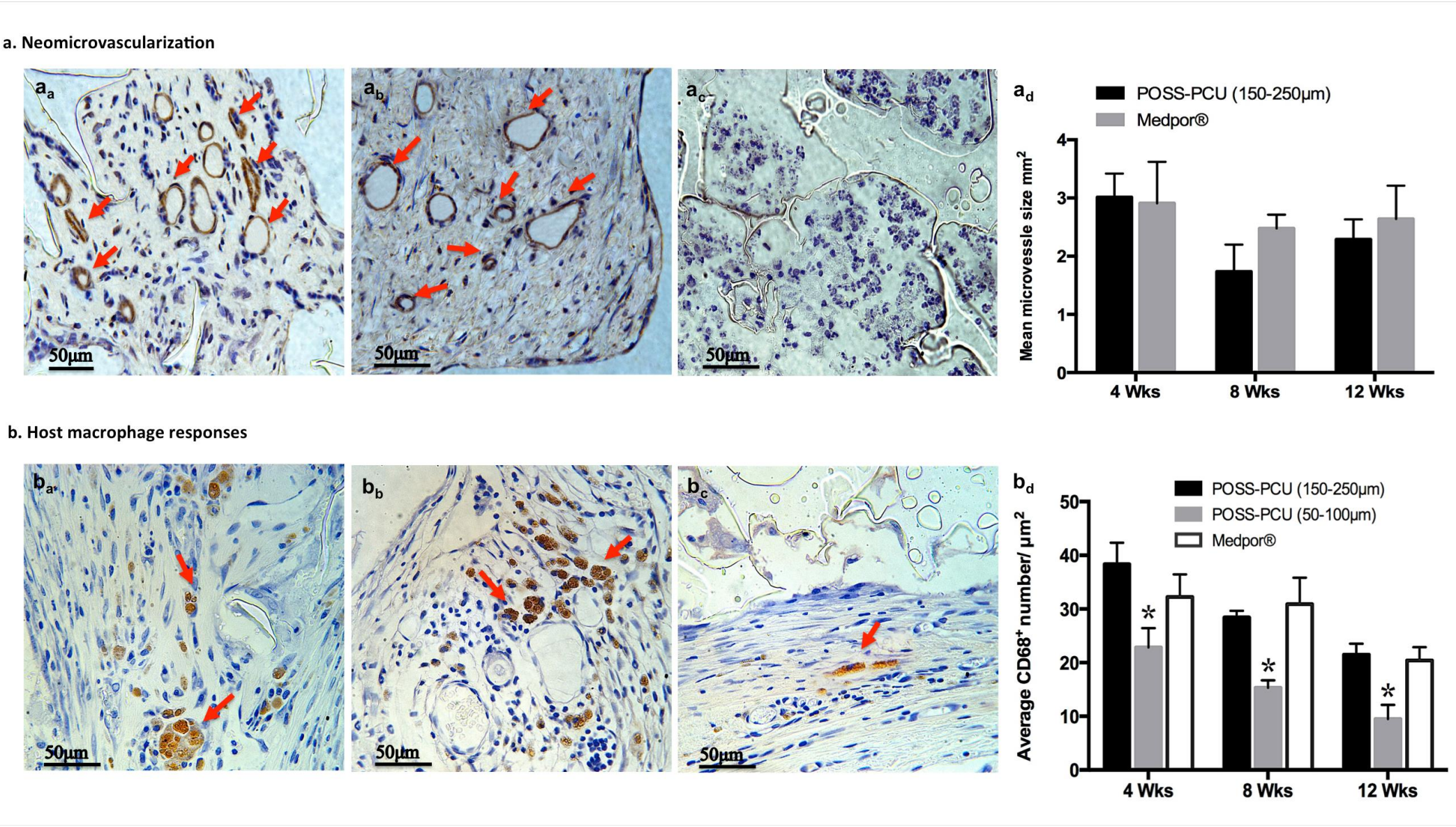
a. Neomicrovascularization
a_a
50μm
a_b
50μm
a_c
50μm
a_d
POSS-PCU (150-250μm)
Medpor®
Mean microvessle size mm²
4
3
2
1
0
4 Wks
8 Wks
12 Wks
b. Host macrophage responses
b_a
50μm
b_b
50μm
b_c
50μm
b_d
POSS-PCU (150-250μm)
POSS-PCU (50-100μm)
Medpor®
Average CD68⁺ number/ μm²
50
40
30
20
10
0
*
*
*
4 Wks
8 Wks
12 Wks

Supplementary Information

Supplementary Experimental Section

Physicochemical characterisation of materials. The surface chemistry, topography, and mechanical properties of the POSS-PCU nanocomposite scaffold (NS) and Medpor® have been previously characterised and the protocols were published in detail.[1] The changes in the pore size of NSs changed the mechanical and total porosity, but not the chemistry. A table summary of the physicochemical properties of these materials was presented (**Supplementary Table 1**).

Table S1. Physicochemical properties of POSS-PCU nanocomposite scaffolds (NSs) and Medpor® used in *in vitro* and *in vivo* studies. *Data obtained from previously published results. [1]

Samples	Average Pore size (μm)	Total porosity (%)+	Youngs modulus (MPa)	Contact angel (captive bubble) (θ)	Mean root square roughness (Rq) (nm)
POSS-PCU*	~150	63.47±1.35	5.73±0.17	53.24±0.13º	82.2±11.8
POSS-PCU (NS1)	50-100	57.04±1.15	5.84±0.23	53.24±0.13º*	82.2±11.8*
POSS-PCU (NS2)	150-250	69.70±1.42	4.09±0.29	53.24±0.13º*	82.2±11.8*
Medpor®*	>100	50	140.9±0.04	45.67±0.23º	119.0±13.8

Rq indicates mean root square roughness; Values are mean±SD, (n=4).
+Weight ratio of porogen particles to POSS-PCU was 3:7 for all NS samples.
* Youngs modulus of human auricular cartilage was 5.02±0.04 (MPa), respectively.

In vitro biological interactions

Fibroblast culture. Human dermal fibroblast (HDF) cell derived from the dermis of normal human neonatal foreskin or adult skin (ECACC, UK, Number 06090715), were cultured in Dulbecco's modified Eagle's medium (DMEM) supplemented with 10% foetal bovine serum (FBS) and 1% antibiotic (50 μg/mL streptomycin, 50 U/mL penicillin) solutions (all from Invitrogen, UK) and incubated at 37 ◦C. The 16 mm polymer discs (n=4) were autoclaved, washed in sterile phosphate-buffered saline (PBS) and pre-incubated in 1 ml of supplemented

culture media for 24 h overnight. Each polymer disc was seeded with cells at a density of 4 x 10^4 cells/cm^2 in 1 ml of cell culture medium. Media were replaced every two days.

Macrophage culture. The human promonocytic cell line U937, isolated from a histiocytic lymphoma (ECACC, UK, Number 85011440), were cultured in RPMI-1640 supplemented with 10% foetal bovine serum (FBS), 5% L-glutamin (2mM) and 1% antibiotic (50 μg/mL streptomycin, 50 U/mL penicillin) solutions (all from Sigma, UK) and incubated at 37 °C under a humidified atmosphere of 5% CO_2. The non-adherent undifferentiated U937 washed (x3) every 3-4 days in Hank's balance solution. The 16 mm polymer discs (n=4) were autoclaved and washed in sterile PBS, and pre-incubated in 1 ml of supplemented culture media for 24 hrs overnight. Each polymer disc in 24 well plate was seeded with U937 cells at a density of 1 x 10^5 cells/cm^2 in 1 ml of cell culture medium supplemented with 0.5 nM phorbol-12-myristate 13-acetate (PMA) (Sigma, UK). Under these conditions, U937 monocytes will adhere to surfaces and differentiate into macrophage-like cells. After 24 hrs the wells were aspirated to remove any unattached, and non-differentiated monocytes, and replaced with fresh medium. Lipopolysaccharide (LPS), a gram-negative bacterium, (Sigma, UK) stimulated transformed macrophages on the polymer surfaces at a concentration of 1 μg/ml as positive control.

DNA content quantification via Total DNA Hoechst staining. Briefly, cells were lysed (x3) using freeze-thaw cycles following the removal of cell culture supernatants stored froze. Lysed cells were stored in a freezer at -80°C and thawed to room temperature. The lysate were incubated with molecular biology grade water (Sigma, UK) for 1 hr in each cycle and Hoechst stain was added at a final concentration of 2μg/ml. The fluorescence of Hoechst dye was measured at 360 nm excitation wavelength and 460 nm emission wavelength using a fluorescence microplate reader (Fluoroskan Ascent FL, Thermo Labsystems, UK). Total

DNA and cell number standard curves were obtained from serial dilutions of known DNA concentrations (positive control) (calf thymus, Sigma, UK) and different cell densities, respectively.

Cell metabolism via Alamar Blue® (AB) assay. Briefly, 10% (v/v) of AB (100 µl/mL solution of AB in DMEM) was added to the culture media of the cell-seeded polymer discs 4 hrs prior to the end of cell culture. Aliquots (100 µl) were placed in a 96 well plate, and the absorbance read on a fluorescence plate reader (Fluroskan Ascent FL reader, Thermo Labsystems, Basingstoke, UK) at 530 nm excitation wavelength and 620 nm emission wavelength.

Total Extracellular Collagen production via Hydroxyproline assay. The measurement of hydroxyproline residues needed for stabilization of the collagen triple helix, known as procollagen, was used as a relevant marker for total amount of secreted collagen from cell cultures. Hydroxyproline is a non-proteinogenic amino acid, which results from the hydrolysis of all types of collagen present in the sample, without discriminating between collagen, insoluble, cross-linked collagen, and soluble collagen. Briefly, the supernatant (250 µl) of each sample was acid hydrolysed in 12M hydroxyl chloride (HCl) at 90 °C for 20 hours, diluted at least twofold using 4M HCl, centrifuged each for 10 min at 13,000 (xg), and analysed for hydroxyproline using a colorimetric kit, according to the established protocol. The diluent sample (35 µl) was dispensed into 96-well plates, added with assay buffer (75 µl), and incubated at room temperature for 20 min. After that 75 µl of detection reagents was placed in each well for 60 min at 60 °C. The absorbance eluted stain was measured at 570 nm in a microplate reader (Anthos 2020 microplate reader, Biochrome Ltd, UK) and the amount of soluble and insoluble collagen estimated. Results were calculated by interpretation from a standard curve obtained from serial dilutions of hydrolysis rat-tail collagen standard (positive control), following manufacturer's instructions.

Vascular endothelial growth factor (VEGF) production. The concentration of VEGF was quantified using a sandwich enzyme linked immunosorbent assay (ELISA) kit following the manufacturer's protocol. Briefly, cell culture supernatants seeded on each polymer surface were centrifuged at 200g for 10 min and aliquoted and stored at –20 ºC. A monoclonal antibody specific for VEGF had been pre-coated onto the ELISA 96 well micro-plate. The supernatants from each sample (duplicated of 200 µl) were pipetted into these wells and incubated for 2 hrs at room temperature, any VEGF present were bound to the immobilised anti-VEGF antibody. After aspirating and washing an enzyme linked anti-VEGF polyclonal antibody is added to the wells (200 µl for 2 hrs at room temperature), followed (after washing) by the addition of the substrate solution (200 µl) and incubated for 20 min at room temperature. The colour develops proportionally to the amount of VEGF present. The colour development was stopped (50 µl of stop solution R&D) and the colour intensity measured with a colorimetric plate reader (Anthos 2020 microplate reader, Biochrome Ltd, UK) at 450 nm with a wavelength correction of 540 nm within 10 min of addition of stop solution. Results were calculated by interpolation from a standard curve obtained from serial dilutions of known human recombinant VEGF (positive control), according to manufacturer's instructions. This assay detects human VEGF164 (the predominant isoform) with a sensitivity of 5 pg/mL in the range of 15–1000 pg/mL.

Cytokine release. The concentration of released cytokines including, interleukin-1 (IL-1β/ IL-1F2), tumour necrosis factor (TNFa/ TNFSF1A), and IL-10 were determined using specific ELISA kits following the manufacturer's protocols. Briefly, cell culture supernatants seeded on each polymer surface were centrifuged at 200g for 10 min and aliquoted and stored at –20 ºC. A monoclonal antibody specific for each cytokines had been pre-coated onto the ELISA 96 well micro-plate. The supernatants from each sample (duplicated of 200 µl) were pipetted into these wells and incubated for 2 hrs at room temperature, any related specific

cytokines present bound to the immobilised anti-related cytokine antibody. After aspirating and washing an enzyme linked anti-related cytokine polyclonal antibody is added to the wells (200 µl for 1 hr at room temperature), followed (after washing) by the addition of the substrate solution (200 µl) and incubated for 20 min at room temperature. The colour develops proportionally to the amount of related cytokine present. The colour development was stopped (50 µl of stop solution R&D) and the colour intensity measured with a colorimetric plate reader (Anthos 2020 microplate reader, Biochrome Ltd, UK) at 450 nm with a wavelength correction of 540 nm within 30 min of addition of stop solution. Results were calculated by interpolation from a standard curve obtained from serial dilutions of each known human cytokines (positive control), according to manufacturer's instructions.

In vivo evaluation

Histology assessments. Following fixation, the length of each post-implantation scaffold was measured in millimeters and sliced horizontally (from top) into ~4 sections of roughly equal thickness in preparation for paraffin wax embedded. Following routine H&E staining on 5-µm sections, the stained samples were observed by using the light microscope (Leitz, Wetzlar, Germany) fixed with a multispectral imaging system (CRi-Nuance™ FX, USA), and the percentage volume fraction of fibrotic tissue (VF) ingrowth within each scaffold for each implantation period was estimate by using an ImageJ software, version 1.47 (National Institute of Health, USA) technique of area counting covered with ingrown fibrotic tissue. Connective tissues enmeshed with spindle-shaped fibroblasts were considered as an ingrown fibrous tissue; while round-shaped cells and rare spindle-shaped fibroblasts in the most inner area were considered as non-ingrown fibrovascular tissues as previously described.[2] All estimations were analyzed at a final magnification of 4× and 24 fields of view for each scaffold (n=4). The area of tissue ingrowth was measured at three different areas evenly

distributed in each of the 2 middle-area of scaffold sections (~ depth 6mm from the external surface of the implant edge to central end point of ingrowth) for each scaffold. Briefly, area test points were randomly superimposed onto the surface of each imaged scaffold section, and the area of test points overlying tissue ingrowth were counted for each evenly random selected field of view. The sum of all area points hitting the tissue ingrowth was divided by the sum of all points hitting the scaffold area over all fields analyzed, generating a percentage volume fraction of the scaffold occupied by ingrown fibrotic tissue (%VF).

The thickness of the fibrous capsule was measured at a final magnification of 10× and six different points (from the implant margin to the end point of fibrous encapsulation) of each randomly and uniformly selected imaged scaffold sections for each scaffold (n=4). The reported thickness values were indicated using semi-quantitative image analysis using the ImageJ software.

Immunohistochemistry (IHC) assessments. Details of the immunohistochemistry staining protocols for von Wilibrand Factor (vWF) and CD68, respectively, for characterising vascular EC and pan-macrophage/monocyte cell markers were presented **(Supplementary Table 2)**.

Table S2. Pretreatment and dilutions of antibodies for immunohistochemistry labelling of endothelial cells (ECs), and macrophages markers using vWF, and CD-68 staining, respectively.

Antigen Retrieval	Blocking Solution	Primary Antibody	Peroxidase substrate	Secondary Antibody
Proteinase K, PH 7.5, 3-6 min (Dako S3020)	2.5% normal horse serum- 30 min (readymade Vector MP-7401)	Polyclonal rabbit anti-human von Willebrand factor- 2h (vWF A0082, Dako Ab & Dako Ab diluent S0809) **1:50 diluted**	Diaminobenzidine (DAB)- (brown) (Vector SK-4105)	ImmPRESS™ anti-Rabit immunoglobulin- 30 min (readymade Vector MP-7401)
Proteinase K, PH 7.5, 3-6 min (Dako S3020)	2.5% normal horse serum- 30 min (readymade Vector MP-7402)	Monoclonal mouse anti-human CD68, clone MAC387- 2h (anti-L1 Thermo Scientific™, PIMA 133969) **1:100 diluted**	Diaminobenzidine (DAB)- (brown) (Vector SK-4105)	ImmPRESS™ anti-Mouse immunoglobulin- 30 min (readymade Vector MP-7402)

* 3% hydrogen peroxide diluted in Methanol- 30 min (Sigma Aldrich) used to inhibit endogenous peroxidase activity. Hoechst 33258 was used as the nuclear stain. As negative controls, immunohistological stained in the absence of the primary antibody.

Blood vessels formation was identified via immunolocalization with the ECs marker, vWF. The percentage volume fraction of the stained microvasculature within each host tissue of implanted scaffolds (total percentage microvessel area (mm^2)) was estimated by using the previously described technique of area counting overlying small blood vessels for each evenly random selected field of view. All estimations were analyzed at a final magnification of 40× and 32 fields of view for each scaffold (n=4). The volume fraction was considered the main tissue within scaffold related parameter characterizing the extent of neovascularization (reflecting both the number and size of new small blood vessels).

Host macrophage inflammatory response was identified via immunolocalization with the pan-macrophage/monocyte cell marker, CD-68. Immunolabeled sections (5-μm) were used to obtain the average cell counting of CD68 pan-macrophage/ monocyte positive cells within the implants. The stained samples were observed by using the light microscope (Leitz, Wetzlar, Germany) fixed with a multispectral imaging system (CRi-Nuance™ FX, USA) at magnification 40×. An unbiased sampling frame was applied under Image J software control to each uniformly and randomly selected image (field of view). Average cell counting data was obtained on approximately 32 fields of view (25 x 104 μm^2) per scaffold (n=4) by using a uniform random sampling approach.

Supplementary Figure Legends

Figure S2. *In vitro* biological evaluation of HDFs of NS compared to Medpor®. a, A significantly higher collagen production per cell was observed on NS than Medpor® over 3 days , followed by non-significant increase after day 7. b, A significantly higher VEGF release per cell was obtained on Medpor® than NS at 14 days.

Figure S3. *In vitro* inflammatory responses of macrophages of the NSs compared to Medpor®. a_a, No significant difference in total U937 cell number and a_b, in rate of cell proliferation (% of total DNA relate to day 1) was observed on both NS and Medpor® scaffolds over 72 hrs. b_a, and b_b, Scanning electron microscopy (SEM) micrograph images of transformed adhered U937 macrophages with rounded cell morphology (red arrow) after 3 days culture on NS and Medpor®. c_a, and c_c, No significant differences in IL-1β/μg DNA, and IL-10/μg DNA cytokines production was observed on both NS and Medpor® after 72 hrs, apart from c_c, TNF-α/μg DNA that presented a significantly lower production on NS than Medpor®.

Figure S4. *In vivo* nanocomposite scaffold microstructure. SEM images of the cross-sectional of POSS-PCU (50-100μm; NS1) and POSS-PCU (150-250μm; NS2). The pore size is correlates closely with porogen particular size as expected.

Figure S5. *In vivo* neovascularisation and host macrophage responses evaluation of the NSs implants compared to Medpor®. a, Number of microvessel/mm^2, and b, total percentage microvessel area (mm^2) in large pore sizes of NS and Medpor®, representing the number, and volume of occupied blood vessels within grown tissue per scaffold, as quantified at 4, 8, and 12 wks, with no observable significant differences between the groups.

Reference List

[1] L. Nayyer, M. Birchall, A. M. Seifalian, G. Jell, *Nanomedicine*. **2014**, *10*, 235.

[2] P. A. Rubin, T. E. Nicaeus, M. A. Warner, H. D. Remulla, *Ophthal. Plast. Reconstr. Surg.* **1997**, *13*, 8.

Figure S2.

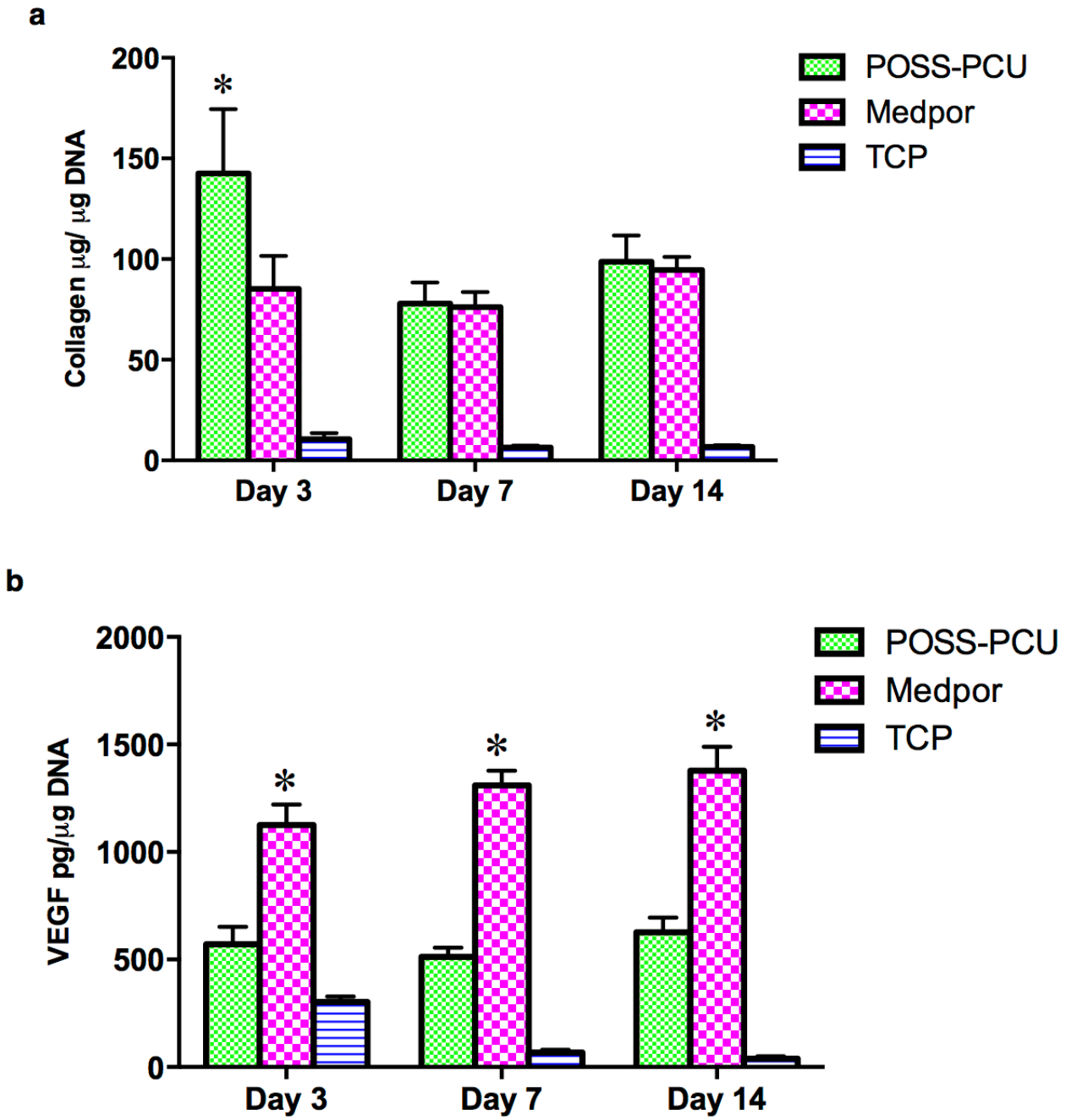
a
Collagen μg/ μg DNA
200
150
100
50
0
*
Day 3
Day 7
Day 14
POSS-PCU
Medpor
TCP
b
VEGF pg/μg DNA
2000
1500
1000
500
0
*
*
*
Day 3
Day 7
Day 14
POSS-PCU
Medpor
TCP

Figure S3.

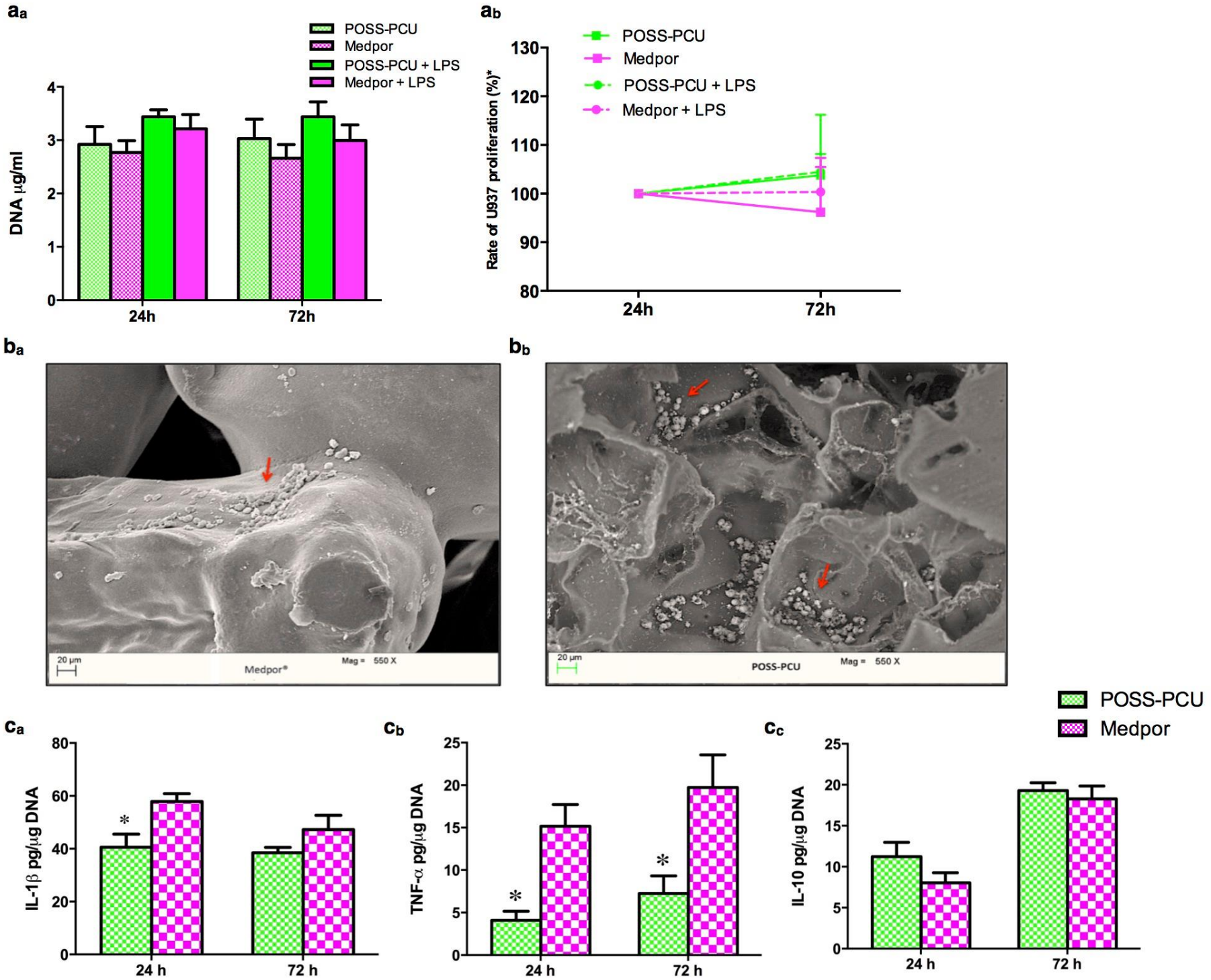
a_a
POSS-PCU
Medpor
POSS-PCU + LPS
Medpor + LPS
DNA µg/ml
0
1
2
3
4
24h
72h
a_b
POSS-PCU
Medpor
POSS-PCU + LPS
Medpor + LPS
Rate of U937 proliferation (%)*
80
90
100
110
120
130
24h
72h
b_a
20 µm
Medpor®
Mag = 550 X
b_b
20 µm
POSS-PCU
Mag = 550 X
c_a
IL-1β pg/µg DNA
0
20
40
60
80
*
24 h
72 h
c_b
TNF-α pg/µg DNA
0
5
10
15
20
25
*
*
24 h
72 h
c_c
IL-10 pg/µg DNA
0
5
10
15
20
25
24 h
72 h
POSS-PCU
Medpor

Figure S4.

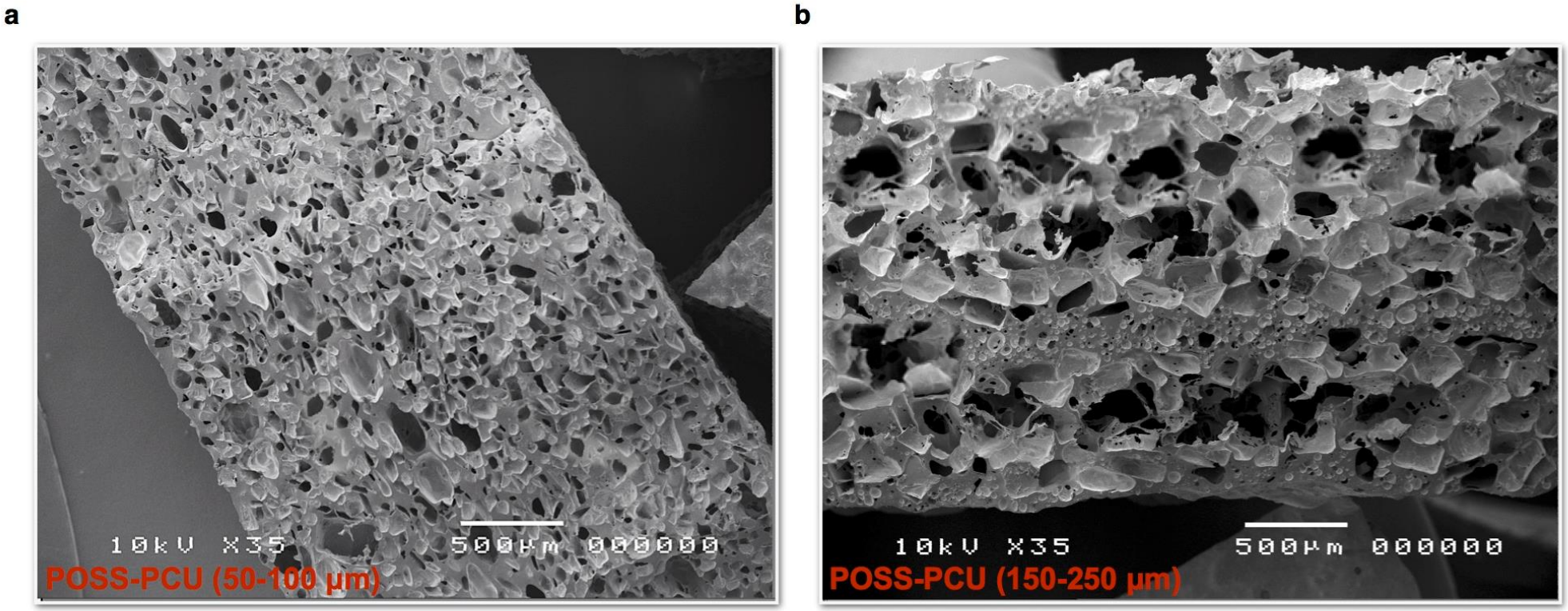
a
10kV X35
500µm 000000
POSS-PCU (50-100 µm)
b
10kV X35
500µm 000000
POSS-PCU (150-250 µm)

Figure S5.

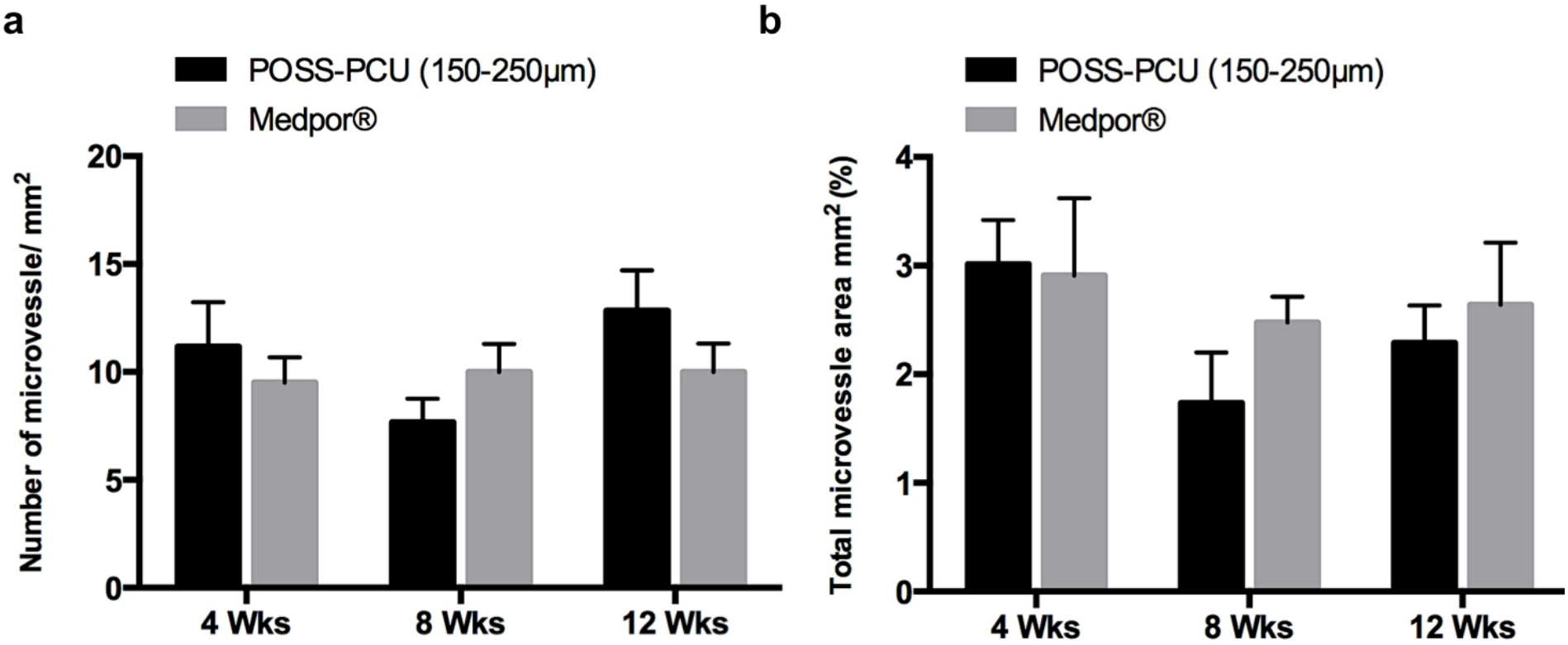
a
POSS-PCU (150-250μm)
Medpor®
Number of microvessle/ mm2
20
15
10
5
0
4 Wks
8 Wks
12 Wks
b
POSS-PCU (150-250μm)
Medpor®
Total microvessle area mm2 (%)
4
3
2
1
0
4 Wks
8 Wks
12 Wks